Article:
Mercuri, M., Wustmann, K., Tengg-Kobligk, H.V. et al. (3 more authors) (2020) Subject-specific simulation for non-invasive assessment of aortic coarctation: Towards a translational approach. Medical Engineering and Physics. ISSN 1350-4533

https://doi.org/10.1016/j.medengphy.2019.12.003

Subject-specific simulation for non-invasive assessment of aortic coarctation: towards a translational approach

Massimiliano Mercuri[a,b], Kerstin Wustmann[c], Hendrik von Tengg-Kobligk[d], Cemil Göksu[d], D Rodney Hose[d,f], Andrew Narracott[d,e]

[a]*Mathematical Modelling in Medicine Group, Department of Infection, Immunity and Cardiovascular Science, University of Sheffield, Sheffield, United Kingdom.*
[b]*Therenva , Rennes , France.*
[c]*Center for Congenital Heart Disease, Cardiac Magnetic Resonance Imaging, Department of Cardiology, University Hospital Bern, Bern, Switzerland.*
[d]*Department of Diagnostic, Interventional and Pediatric Radiology, University of Bern, Bern University Hospital, Bern, Switzerland*
[e]*INSIGNEO Institute for in Silico Medicine, The University of Sheffield, Sheffield, U.K.*
[f]*Department of Circulation and Medical Imaging, NTNU, Trondheim, Norway*

Abstract

We present a multi-scale CFD-based study conducted in a cohort of 11 patients with aortic coarctation (CoA). The study explores the potential for implementation of a workflow using non-invasive routinely collected medical imaging data and clinical measurements to provide a more detailed insight into local aortic haemodynamics in order to support clinical decision making. Our approach is multi-scale, using a reduced-order model (1D/0D) and an optimization process for the personalization of patient-specific boundary conditions and aortic vessel wall parameters from non-invasive measurements, to inform a more complex model (3D/0D) representing 3D aortic patient-specific anatomy. The reliability of the modelling approach is investigated by comparing 3D/0D model pressure drop estimation with measured peak gradients recorded during diagnostic cardiac catheterization and 2D PC-MRI flow rate measurements in the descending aorta. The current study demonstrated that the proposed approach requires low levels of user interaction, making it suitable for the clinical setting. The agreement between computed blood pressure drop and catheter measurements is 10 ± 8 mmHg at the coarctation site. The comparison between CFD derived and catheter measured pressure gradients indicated that the model has to be improved, suggesting the use of time varying pressure waveforms to further optimize the tuning process and modelling assumptions.

Keywords: haemodynamics, subject-specific modelling, magnetic resonance imaging, aortic coarctation, multi-scale models, computational fluid-dynamics

words count: 4868.

1. Introduction

Coarctation of the Aorta (CoA) is a Congenital Heart Disease (CHD) accounting for 5-8 % of all congenital cardiac defects [1, 2], it is the fifth most common CHD [3].
CoA is characterized by a localized stenosis of the descending aorta, in most cases located after the origin of the left subclavian artery (patent ductus arteriosus region). The obstruction alters blood pressure distribution and perfusion, causing upper body and cerebral hypertension, left ventricular hypertrophy with diastolic and later systolic dysfunction, coronary artery disease, cerebral haemorrhage, stroke and aortic ruptures [4, 5]. Patients with untreated coarctation have an average survival age of 35 years, with 75 % chance of dying by 46 years of age [6, 7].
Treatments include surgical repairs, stent implantation and balloon angioplasty [8]. Current guidelines recommend intervention if the peak-to-peak coarctation gradient (the difference in peak pressure at the proximal aorta and beyond the coarctation site) exceeds 20 mmHg at rest [6]. In clinical practice, invasive cardiac catheterization is considered the gold standard for the assessment of trans-coarctation gradient. Despite its accuracy, the technique is an invasive method with rare but potential complications. Trans-coarctation gradient can be estimated non-invasively from arm/leg blood pressure measurements or from imaging methods, such as Doppler ultrasound (DUS) or phase contrast magnetic resonance imaging (PC-MRI). From imaging data, the pressure drop over the stenosis is derived from a simplified Bernoulli's equation with measured peak velocity provided as input [9, 10]. Both techniques have been shown to provide good overall correlation with invasive cardiac catheterization peak-to-peak measurements, but in many cases overestimate this value since they do not take into account for unsteady and viscous losses, velocity profile contribution on pressure decay and pressure recovery effects downstream of the coarctation [11, 12].
With the advance of Computational fluid dynamics (CFD) it has been possible to improve the non-invasive estimation of the peak-to-peak pressure gradients with patient-specific model, derived from imaging data. Several computational studies have been published in the last decade focused on subject-specific CoA cases. They differ in the approaches used to model haemodynamics, the representation of aortic distensibility and the strategies used to derive boundary con-

ditions (BCs) from the available clinical data. The computational problem has been approached using both three-dimensional (3D) models [13–22] and one-dimensional (1D) models [23, 24], with a range of different assumptions: rigid [13, 16, 18–21] or deformable walls [14, 15, 17, 22–24], simple BCs such as literature derived flow-split conditions [18, 19], flow-split conditions together with time-varying clinically measured pressure waveforms [13, 22] or more complex BCs such as coupled (0D) Windkessel models to represent the circulation beyond the local aortic region [14–17, 20, 21, 23, 24]. The flow-split assumption provides a fast and easy way to model the outlet flow distribution but lacks realism since flow rate is assumed to a have a constant ratio over the cardiac cycle; patient-specific pressure or flow rate waveforms can be applied at each outlet but they are not often routinely collected. Although more complex, Windkessel models improve the accuracy of outlet models whilst requiring relatively little clinical data, nonetheless the tuning process of Windkessel parameters can be a time-consuming task, especially if performed iteratively using 3D models.

In this article, we describe a computational workflow that, from non-invasive data typically available for all CoA patients, offers a detailed insight into the local aortic fluid-dynamics. The final aim of this work is to provide computational clinical decision support that can be integrated within an existing commercial software framework (Endosize) developed by Therenva (Rennes, France).

First, we describe the clinically available patient-specific data collection and processing. Next, we describe the 1D/0D and 3D/0D model set-up followed by the tuning process used to obtain parameters for the 0D components. When compared with the literature, the approach used in this work represents aortic haemodynamics using multiple geometrical modelling approaches to automatically tune Windkessel boundary conditions from available clinical data. Data processing of model outputs is described followed by results, including comparison between predicted and measured pressure gradient across the coarctation and descending aortic flow rate. The discussion focusses on potential future application of the workflow within the clinical setting and comparison with previously reported approaches.

2. Materials and Methods

*2.1. **In vivo data: acquisition and model generation***

This section details the analysis of clinical data obtained from 11 patients undergoing assessment of severity of aortic coarctation. The cohort was heterogeneous and included patients who had already undergone coarctation repair (see Table 1). The clinical data collected includes contrast-enhanced magnetic resonance angiography (CE-MRA) images of aortic geometry, two-dimensional phase contrast magnetic resonance imaging (2D PC-MRI) measurement of aortic flow rate in the ascending and descending aorta (proximal and distal to the coarctation site), cuff pressure measurements from the right arm and at the foot. All data were collected at Bern University Hospital, following a protocol approved by the local ethics committee and the volunteers provided written informed consent (Swiss Adult Congenital Heart disease Registry, SACHER, ClinicalTrials.gov Identifier NCT 02258724).

2.1.1. Aortic geometry

A contrast-enhanced magnetic resonance angiography (CE-MRA) was performed as a first assessment for clinical suspicion of aortic coarctation or as a follow-up exam after previous surgical intervention for all 11 patients.

The subjects were scanned in the supine position with a 1.5T MAGNETOM Aera scanner (Siemens Healthcare, Erlangen, Germany) using a T1 weighted, k-space, spoiled gradient recalled echo sequence (echo time: 1.1 ms , repetition time: 3.17 ms , flip angle: 30° , field of view: 370-420 mm, slice thickness: 1-1.2 mm, acquisition matrix: 384 x 250 reconstructed to 512 x 512) and an intravenous Gadolinium-based contrast medium injection with optimal contrast timing to enhance the thoracic aorta (contrast flow at 3.5 ml/s) through the test-bolus technique (see Figure 1 (a)).

The 3D geometry was then reconstructed using a semi-automatic segmentation software (Philips Intellispace, Philips, Koninklijke, Netherlands) to provide geometry in the form of an STL file (see Figure 1 (b)). The STL file was post-processed manually using the open source software Autodesk MeshMixer (Autodesk, Inc). The final STL was truncated to obtain four outlets (cutting the surface perpendicular to the extracted centerline) using the vmtk toolkit [25] as shown in Figure 1 (c). The typical geometry processing time is less than 15 minutes.

2.1.2. Aortic flow rate

Volume flow rate waveforms were obtained at two planes perpendicular to the aorta: at the ascending aorta at the level of the right pulmonary artery and at the descending aorta at the diaphragmatic level, using retrospectively ECG-triggered 2D PC-MRI data (echo time: 2.47 ms , repetition time: 37.12 ms , flip angle: 20° , field of view: 320-370 mm, slice thickness: 6 mm, acquisition matrix: 192 x 119, velocity encoding 150-200 $cm \cdot s^{-1}$, temporal resolution 30 phases/cardiac cycle).

2.1.3. Patient-specific coarctation pressure drop

Resting blood pressure cuff measurements were taken at the right arm and at the leg as reported in Table 2 using an appropriately sized sphygmometer cuff. Right cubital blood pressure was measured using an automatic oscillometric method (Dinamap Procare 300, GE Healthcare) after resting for more than 5 minutes. Systolic blood pressure in one of the legs (dorsalis pedis artery or posteria tibial artery) was measured by an appropriately sized cuff placed around the lower calf and using a Doppler probe (Huntleigh dopplex D900, Huntleigh Healthcare Ltd, Cardiff, UK).

Mostly, blood pressure measurements were performed either simultaneously at the arm and the leg, or within 3 minutes of each other. Blood pressure difference was calculated between the proximal (arm) and distal (leg) systolic blood pressure. All non-invasive blood pressure data were obtained during routine clinical follow-up visit in a centre for congenital heart disease.

Diagnostic catheterization to assess invasive aortic pressure gradients was performed in order to evaluate the need for intervention. Invasive blood pressure curves in the ascending and descending aorta were obtained either simultaneously with the insertion of two catheters (5 French, Cordis, Cardinal Health, US) using a radial and femoral arterial access or by pullback technique using one catheter. All measurements were collected over 5 cardiac cycles and the peak-to-peak pressure gradient was calculated by the integrated pressure monitoring system (Siemens Healthcare, Erlangen, Germany). The computational models were not informed by catheter-based pressure measurements and the peak-to-peak measurement was used only for validation to compare with the simulation results.

2.2. Modelling approach

Two distinct models were informed by the available clinical dataset. The first model was a 1D/0D numerical model and the second a 3D/0D numerical model. In this section the formulation of these two models is provided, together with a description of the required physical and geometrical input parameters and the simulated quantities that are relevant for this study.

2.2.1. One-dimensional formulation

In the 1D/0D modelling framework, the aortic geometry was divided into a series of interconnected segments. For each segment a system of one dimensional nonlinear hyperbolic equations was defined, derived from the continuity and Navier-Stokes equations for incompressible flow within a deformable elastic vessel [26], as follows

$$\begin{cases} \frac{\partial A}{\partial t} + \frac{\partial Au}{\partial x} = 0, \\ \\ \frac{\partial u}{\partial t} + u\frac{\partial}{\partial x}(u) + \frac{1}{\rho}\frac{\partial P}{\partial z} = \frac{f}{\rho A}, \\ \\ P = P_{ext} + \beta\Big[\sqrt{\frac{A}{A_0}} - 1\Big],\ \beta = \sqrt{\frac{\pi}{A_0}}\frac{Eh_0}{1-\nu^2}, \end{cases} \tag{1}$$

where t is the time, x is the axial coordinate along the vessel, $A(x,t)$ is the cross-sectional area of the vessel lumen, A_0 is the reference cross-sectional area (when $P = P_{ext}$), h_0 is the reference wall thickness, $u(x,t)$ and $P(x,t)$ are the axial blood velocity and blood pressure averaged over the cross-section, ρ is the density of blood assumed constant, while $f(x,t)$ is the frictional force per unit length.

The frictional losses were computed by assuming a flat velocity profile (the corresponding Womerlsey numbers derived at the inlet of the aorta varies from 11 to 30) with a polynomial order of 9 ($\zeta = 9$) with

$$f = -2 \cdot (\zeta + 2) \cdot \mu \cdot \pi \cdot u(x,t) \tag{2}$$

where μ is the viscosity of blood. This assumption provides best fitting when compared to experimental results in a human arterial tree [27]. Following this assumption the momentum correction factor (or Coriolis coefficient) was set constant in time and space and equal to 1 [28].

The system of equations in (1) was solved using a finite-volume numerical scheme formulation provided by Melis et al. [26]. For all the simulations, the density and viscosity of blood were assumed constant ($\mu = 4.5\ mPa \cdot s$ [24] and $\rho = 1060\ kg \cdot m^{-3}$).

The stability of the scheme was guaranteed by the computation of the time step for each iteration in all vessels depending on their maximum local wave speed c_{max} and the element length Δx as

$$\Delta t = C_{cfl} \cdot \frac{\Delta x}{c_{max}} \tag{3}$$

where the Courant number was set to $C_{cfl} = 0.9$ and Δt was set to the smallest computed value over all elements.

2.2.2. Three dimensional formulation

The Navier-Stokes (NS) and continuity equations were solved in 3D over time using a transient analysis with the finite volume CFD-based solver ANSYS-FLUENT 17.2 (ANSYS Inc., PA, USA). Local aortic distensibility was included using a compressible fluid strategy as described by Brown et al. [29]. Blood density changes were related to pressure changes via an ideal gas with the fluid wave speed, c, as input. The inflow boundary condition was provided by imposing the time-varying mass flowrate waveform at the inlet (assuming a flat velocity profile and an initial density of $1060\ kg \cdot m^{-3}$). The viscosity of blood was set equal to $\mu = 4.5\ mPa \cdot s$ using a Newtonian model. The simulation was run with a laminar flow model, the cases were peak Reynolds numbers at the coarctation site exceeded the limit imposed by the classical turbulence analysis (3500) were recomputed using an SST turbulence model. The solution was performed using a double precision solver with a second order discretization coupled scheme for pressure-velocity coupling and a time step of $10^{-4} s$ to ensure convergence over the entire cardiac cycle. Simulations were run for three to five cardiac cycles until the mass flow rate and pressure fields yielded consistent solutions over successive cycles (change in peak pressure and mass flow rate less than 1 %).

2.3. Three-dimensional and one dimensional meshes

For the three-dimensional model, the mesh was generated with FLUENT automatic mesh library starting from the STL file using polyhedral elements with 5 prism layers at the wall. The number of elements varied from 105205 to 564822 element volumes and edge lengths varied from $3.00 \cdot 10^{-13}\ m^3$ to $1.71 \cdot 10^{-9}\ m^3$ and from $6.93 \cdot 10^{-5}\ m$ to $2.94 \cdot 10^{-4}\ m$, respectively.

For the 1D model formulation the vessel centerlines were extracted from the STL files using vmtk libraries and tools [25]. Four centerlines were extracted: through the aorta itself and the three supra-aortic vessels: the brachio-cephalic artery (BCA), the left common carotid artery (LCA) and the left-subclavian artery (LSUB). Along these vessel centerlines the perpendicular vessel cross-section was computed every 5 mm (see Figure 1 (e)), defining the vessel segments for the 1D formulation. For each vessel segment the finite volume mesh was defined with an element length of 1 mm. The 1D/0D model was initialized with the cross-sectional area extracted from the CE-MRA geometry as the luminal area A_d at diastolic pressure P_d, and the initial area A_0 found using the pressure-area relationship (or tube-law) in 1. The wall thickness (h_0) was defined as function of lumen radius (R_0) [30] , as follows

$$\frac{h_0}{R_0} = ae^{bR_0} + ce^{dR_0}, \tag{4}$$

Where a, b,c and d are constants. Young's modulus was defined based on the measured pulse wave velocity (c) derived as described in section 2.4, through the equations

$$c = \sqrt{\frac{\beta}{2\rho\sqrt{A_0}}} A_d{}^{\frac{1}{4}}, \tag{5}$$

and

$$\beta = \sqrt{\frac{\pi}{A_0}} \frac{Eh_0}{1-\nu^2} \tag{6}$$

2.4. Mechanical properties

In both the 3D and 1D models, the mechanical properties for the arterial wall were derived from the estimation of the pulse wave velocity, c. The value of c was assumed to be uniform over the aortic geometry and was derived from the 2D PC-MRI data using the transit-time method (or foot-to-foot method) [31] as follows

$$c = \frac{\Delta x}{\Delta t} \tag{7}$$

where Δx is the distance along the vessel centerline between the proximal plane of the 2D PC-MRI measurement in the ascending aorta at the level of the right pulmonary artery, and the distal plane of the 2D PC-MRI measurement in the descending aorta at the level of the diaphragm;

while Δt is the time taken for changes in the flow waveform to travel from the proximal to the distal location.

This value is determined from the calculation of the foot of the flow rate curves at the ascending and descending aorta. For each flow waveform, the foot is derived from the intersection between the gradient during initial flow increase, defined by a line connecting points at 20% and 80% of the maximum flow rate, and the minimum flow rate (also referred as baseline). This method of assessing aortic compliance accounts for variability in aortic stiffness between measurement points, which would not be captured by a local measure of distensibility based on local changes in aortic area and pressure.

The values of pulse wave velocity obtained are reported in Table 3. For patients 1,4,6 and 7 the resulting pulse wave velocity generated instability in the solution of the 1D model, as a result the pulse wave velocity was increased to ensure convergence of the model over the entire cardiac cycle (see Table 3).

2.5. Boundary conditions:overall approach

The same inflow and outflow boundary conditions were imposed for the 1D and 3D solutions (see Figure 2 (b) and Figure 2(c)). At the inlet, the aortic flow waveform $Q_{asc}(t)$ measured by 2D PC-MRI was applied using a Fourier Series reconstruction to increase the time resolution. At each of the four outlets, a three-element Windkessel model, representing the downstream vasculature, was coupled as reported elsewhere [29, 32]. These 0D models consist of a proximal resistance Z, in series with a parallel combination of a distal resistance, R and a compliance, C. These parameters were found using an iterative scheme proposed by Xiao et al. [33] (see Figure 2 (a)).

The scheme starts from estimating the total peripheral compliance, C_T, and the total peripheral resistance, R_T, representing the equivalent resistance and compliance of the whole 1D/0D system. Following the process described in 2.5.1 and 2.5.2 below, the values for the Windkessel parameters were derived for all the outlets (ie, BCA, LCA, LSUB and DescAo) of the 1D/0D domain.

To tune the 1D/0D model coupled system was solved with iterative adjustment C_T and R_T to match the pressure at the aortic inlet to the measured systolic and diastolic cuff pressures, P_s and P_d respectively, assuming that the pressure measured at the right arm is equal to the pressure at the ascending aortic root (see Figure 2 (a)).

2.5.1. Calculating the peripheral resistances of the outflow 0D models

The total resistance, R_T, at the outlet of the 1D/0D network was defined as

$$R_T = \frac{P_m}{\bar{Q}_{in}},\ P_m = P_d + \frac{1}{3}(P_s - P_d) \tag{8}$$

where P_m is the mean aortic pressure, P_s and P_d are the systolic and diastolic cuff pressures, respectively, while $\bar{Q}_{in}$ is the mean aortic flow rate measured at the ascending aorta from 2D PC-MRI data. The total resistance is then distributed over the outlets of the model as follows

$$R^j_{tot} = Z^j + R^j = R_T \frac{\bar{Q}_{in}}{\bar{Q}^j_{out}} \tag{9}$$

where $j = 1, 2, 3, 4$ refers to the four outlet interfaces of the 1D/0D multiscale model (BCA, LCA, LSUB and DescAo), while $\bar{Q}^j_{out}$ is the mean aortic flow rate at the outlet j. The values for $\bar{Q}^j_{out}$ were assumed to be proportional to the square of the radius [34] of each the supra-aortic vessels as follows

$$\bar{Q}^j_{out} = \bar{Q}_i \cdot \frac{r_i^2}{\sum_{i=1}^{i=3} r_i^2} \tag{10}$$

where r_i is the radius of the supra-aortic branch $i = 1, 2, 3$ (ie, BCA, LCA and LSUB) and $\bar{Q}_i$ is the total mean flow rate for the supra-aortic branches, obtained from the difference between the mean aortic flow of the inlet and the mean aortic flow of the descending aorta, derived from the time average of the 2D PC-MRI flow waveform measurements. The proximal resistances, Z^j , at the four outlets (ie, BCA, LCA, LSUB and DescAo) were assumed to match the characteristic impedance of the terminal vessel j, in order to minimize artificial wave reflections, as described elsewhere [35]. For a new iteration $n + 1$, R_T is updated via a first-order Taylor expansion of (8) around the measured diastolic pressure P_d as follows

$$R^{n+1}_T = R^n_T + \frac{\Delta P^n_m}{\bar{Q}_{in}},\ \Delta P^n_m = P_d - P^n_d \tag{11}$$

2.5.2. Calculating the the peripheral compliances of the outflow 0D models

The total compliance,C_T, was calculated as in [36]

$$C_T = \frac{Q_{max} - Q_{min}}{P_s - P_d}\Delta t \tag{12}$$

where Q_{max} and Q_{min} are the maximum and minimum ascending aortic flow rate values, Δt is the time delay between Q_{max} and Q_{min}, and P_s and P_d are the systolic and diastolic cuff pressures, respectively.

Following the work of Alastruey et al. [36] the total compliance, C_T, is equivalent to the sum of the compliance 0D Windkessel elements, C_p, and the compliance that given by the sum of all the 1D model segments, C_c, as

$$C_T = C_c + C_p, \tag{13}$$

From Equation (13) the total peripheral compliance of the outflow models can be derived and distributed to the outflow branches in proportion to the flow distribution as reported by Stergiopulos et al. [28]. For a new iteration $n+1$, C_T is updated via a first-order Taylor expansion of (12) around the measured diastolic pressure P_{pulse} as follows

$$C_T^{n+1} = C_T^n + \frac{Q_{max} - Q_{min}}{(P_{pulse}^n)^2} \Delta t \Delta P_{pulse}^n, \quad \Delta P_{pulse}^n = P_{pulse} - P_{pulse}^n \tag{14}$$

The Windkessel parameters for the outlets compliances and resistances found via the 1D/0D models are then applied to the 3D/0D counterparts. The results obtained from the 3D/0D model were compared to the measured data in terms of 2D PC-MRI measured descending aortic waveforms and catheter derived peak-to-peak pressure gradient.

2.6. Severity of the coarctation

For all patients the severity of the coarctation was quantified from the geometrical 3D extracted shape, using the measure reported by Goubergrits and colleagues [19], the degree of stenosis (DS)

$$DS = (1 - \frac{A_{st}}{A_d}) \tag{15}$$

Where A_{st} is the cross-sectional area at the stenosis (the minimum reported value along the vessel's centerline) and A_d is the cross-sectional area measured 150 mm downstream from the ascending aorta.

2.7. Pressure gradients

Coarctation pressure gradients were reported using the 3D/0D model strategy to capture the nature of the complex haemodynamics in the region of the coarctation. A single value was used for clinical assessment, reported as the difference in peak pressure between the waveform measured in the ascending aorta and that measured in the descending aorta. As the simulation provides the pressure waveform simultaneously at all locations, the following values were reported for comparison with the clinical value:

- Difference in peak pressure between ascending (inlet) and descending (outlet) aorta ($Max_{AscAo} - Max_{DescAo}$);
- Maximum instantaneous pressure gradient across the full computational domain over the full cardiac cycle ($Max_{gradient}$);
- Pressure gradient across the full computational domain at peak systole ($Sys_{gradient}$);
- Pressure gradient over the coarctation region at peak systole ($CoA_{gradient}$).

3. Results

3.1. Arterial geometries and flow rates

The arterial geometry was successful segmented for the 11 patients from CE-MRA. The geometries extracted are reported in Figure 3 together with the signal acquired from the 2D PC-MRI at the two different planes. For patient 11 the temporal resolution of the acquired signal was equal to 20 phases per cardiac cycle with an equivalent signal time around 40 ms. For the remaining patients the 2D PC-MRI temporal resolution was equal to 30 phases/cardiac cycle with an equivalent signal time between 30 and 40 ms.

The length of each supra-aortic branch varied due to loss of signal towards the borders of the volume, which may result in reduced accuracy of the segmentation in these regions [23].

The severity of the coarctation is reported in Table 4. For patient 3 the DS value was not reported as this case represents a hypoplastic descending aorta. The mean value of DS was 48 ± 23% in line with previous published works such as Goubergrits et al. [19] 54.8 ± 19.21%, Itu et al. [24] 48.2 ± 7% , Ralovich et al. [23] 41 ± 9.5%.

3.2. Effectiveness of the tuning process

The effectiveness of the 1D/0D tuning process is detailed for the 11 patients in Table 5. The errors between the 1D/0D and 3D/0D solutions and the systolic and diastolic cuff pressure measurements at the aortic inlet are reported as a percentage.

When solving using the 1D model, the tuning process resulted in errors less than 10% for all patients except for patient 5,9 and 10. The highest relative errors were observed in tuning the systolic pressure, while for patient 9 significant error was observed in both systolic and diastolic values. When the solution was re-computed using the 3D approach, the error increased in most cases but remained below beyond the 10% for 6 of the 11 cases. For an example of comparison between the 1D and 3D model tuning see Figure 4.

3.3. Descending aortic flow rate

Figure 5 compares the mass flow rate measured with 2D PC-MRI with that computed by the 3D/0D CFD model at the descending aorta (measured at the diaphragmatic level). The errors are normalized by the peak flow over the cardiac cycle to avoid division by small values, as reported elsewhere [33]. The overall average errors were below 1%. Peak flow was over-estimated by more than 10% for cases 3,4,5,6 and 9.

3.4. Pressure gradients

Pressure gradient measures are reported in Table 6 from the 3D/0D model along with the pressure catheter measurement. From these results it is observed that the CFD derived metric in best agreement with the measured pressure is the CoA gradient catheter data, MB, of -9 mmHg and standard deviation from the mean difference (LOA, upper limit = 10 mmHg, lower limit = -28 mmHg). The absolute error is 10 ± 8 mmHg. However, direct comparison of the peak-to-peak difference in pressure between the ascending and descending aorta is in poor agreement between the CFD derived metric and the catheter reported values.

4. Discussion

This study takes advantage of recent developments in modelling methods to build an engineering workflow for subject-specific modelling of the haemodynamics in a cohort of 11 patients who were assessed both before and after aortic coarctation repair. Key factors for successful

clinical translation of such technologies include the ability to inform the workflow using non-invasive routinely collected clinical data and the feasibility for robust, repeatable application in a clinical environment.

By exercising the workflow on retrospective data acquired using standard clinical protocols, this study demonstrates the feasibility of using only CE-MRA images, flow rate waveforms acquired via 2D PC-MRI and systolic and diastolic cuff pressure values from the right arm, to construct two levels of model with a relatively low level of user interaction. Compared to previous work, the compressible fluid strategy adopted for the 3D/0D multiscale model allows aortic distensibility to be included without the use of a full FSI model, saving computational cost, simulation time and reducing the level of user interaction required to set-up the model.

This is an advance in the current state of 3D model simulation of CoA patients compared with the approach of Goubergrits et al. [18, 19] where, despite the good agreement with catheter data, aortic distensibility and transient effects were neglected.

This study includes patient-specific aortic distensibility informed by 2D PC-MRI data assuming the elastic properties of the aorta were uniform over the 1D/3D region. This is supported by evidence that the use of non-uniform properties may lead to overestimation of the aortic stiffness [37] and it is well suited to deployment of this approach with existing clinical workflows, where 2D PC-MRI flow rate waveforms are typically available at two locations (aortic root and diaphragmatic aorta).

Compared to previous published reports of 3D/0D approaches this study provides a more patient-specific assessment than La Disa et al. [14] and Coogan et al. [15] who both used mechanical properties derived from literature-based data.

Ralovich et al. [23] and Itu et al. [24] used the same approach proposed here (foot-to-foot method) to inform the deformability of a 1D/0D model from 2D PC-MRI. Their model represented the coarctation site with a time constant nonlinear resistance that incorporated the effect of energy dissipation due to turbulence but did not capture the influence of 3D anatomical features such as curvature, bending, bifurcation and tapering. The importance of such effects, especially at systolic phases, are illustrated in Figure 4 (b) where recirculation and helical flow clearly occurs [33]. Furthermore, it is possible that including a nonlinear resistance may result in artefactual pressure/flow wave reflections due to compliance mismatch.

Despite the limitation of 1D approaches to fully capture geometric effects, a 1D/0D multi-scale

model provides a useful tool for tuning outflow boundary conditions and mechanical properties for the 3D model. The automatic tuning process adopted in this study offers the advantages of requiring only systolic and diastolic cuff pressures, diaphragmatic mean flow rate, and pulse wave velocity from 2D PC-MRI as input data. This avoids manual operator tuning that has been adopted in previous studies [14–17]. Alternative approaches have been proposed such as the use of a detailed velocity profile map extracted from 4D flow MRI [18, 19] or UDS [21], or a detailed catheter-derived pressure waveform applied at the domain boundaries [13, 22], but these require data are often not routinely collected in the clinical enviroment.

The 1D model showed some instabilities at lower values of measured wave speed, which limits the robustness of the tuning process. However, it should be noted that the aortic mechanical properties are derived from the wave speed calculation informed by both 2D PC-MRI and geometrical features, both associated with measurement uncertainties. The 1D/0D tuning process was successful in most cases and the 3D/0D models, with the tuned Windkessel parameters, captured the systolic and diastolic cuff pressure measurements reasonably well. Tuning through iterative solution of the coupled 3D/0D system is possible but introduces very highly computational costs. All 1D simulations were solved on an Intel Xeon E5-1620, 8 cores, 16 GB RAM and took maximum 30 minutes per cardiac cycle. 3D simulations were run using a workstation with 3 processor Intel E5-620 and 12 GB of RAM and took a minimum of 12 hours to a maximum of 22 hours.

The computational method underestimates measured catheter gradients compared with previous published studies [13, 19, 23, 24]. These increased errors may partially arise from the clinical data acquisition process, as data were processed retrospectively and not specifically for this computational study.

The pressure gradient across the coarctation at peak flow provides an assessment of the potential for reduction of the flow limiting effect of the coarctation following treatment, an advantage of the computational approach is the ability to examine this effect in isolation. Due to delayed augmentation in pressure in the descending thoracic aorta predicted by the CFD approach in several cases agreement between peak-to-peak measures of pressure gradient is poor. This suggests that, in addition to measurement errors previously discussed, assumptions made in the general nature of the tuning approach (i.e. distribution of resistance and compliance based on generic relationships based on vessel radius) may lead to poor representation of patient-specific pressure

transmission between the local 3D domain and the Windkessel outlet conditions. A more detailed understanding of these effects would be provided by analysis of the time varying form of the pressure catheter measurements used to provide the clinical peak-to-peak pressure gradient, which was not available during this study.

Several limitations are associated with routine imaging and pressure measurement as aortic imaging by MR, non-invasive blood pressure measurements and invasive measurements by catheterization are typically not performed simultaneously. Furthermore, catheter measurements were performed at rest but without sedation and the location of 2D PC-MRI measurements may be different from that at which the catheter data were obtained. All these limitations may contribute to variability between the model and measured results.

In this study, the effects of collateral flow (due to vertebral, internal mammary, intercostal or collateral arteries that join the descending thoracic aorta distal to the coarctation site) have been neglected because it has not been possible to segment these vessels for all patients, due to the small size of these vessels and limited spatial resolution of MR angiography. Some studies have included such vessels in their models [14, 15] but only starting from the native supra-aortic branch point to the conjunction at the coarctation site without the need for supplementary BCs.

At supra-aortic branches (BCA, LCA, LSUB arteries) no 2D PC-MRI flow rate (as in the case of LaDisa et al. [14]) nor catheter/tonometry derived blood pressure measurements (as described in the work of Alastruey et al. [37]) were available therefore the mean flow rate was imposed based on radii of the vessels, consistent with the report by Zamir et al. [34]. This may introduce some limitations in this study, but the automatic process described here can be simply adapted for future applications if such measurements are routinely acquired.

It should be noted that the same uniform aortic compliance was used for both patients after coarctation repair and unrepaired cases. The possible interaction between the rigid patch (in one patient) and the end-to-end anastomosis and the native aortic wall is expected to increase the number of reflected waves towards the proximal aorta, thus increasing the pressure gradient. In literature, this mechanism has been investigated for CoA patients treated with an aortic stent placement, by increasing the mechanical stiffness of the stented region up to 15 times the normal aortic compliance [15, 23].

This study was conducted using retrospectively collected data obtained from patients at rest, which is likely to increase the uncertainty associated with comparison between CFD and mea-

sured data, in previous research studies under stress conditions the pressure gradient has been shown to reach values above 40 mmHg [22]. However, the rest condition represents the clinical protocol for assessment of coarctation patients under current guidelines [6].

5. Conclusion

This study has demonstrated the feasibility of constructing a workflow using non-invasive routinely collected clinical data to predict the pressure gradient in coarctation patients using patient specific CFD simulation, with relatively low levels of user interaction required. Further work is required to enhance the tuning process to improve agreement with measured catheter data.

6. Acknowledgements

This project has received funding from the European Union's Horizon 2020 research and innovation programme under the Marie Sklodowska-Curie grant agreement no. 642612, VPH-CaSE (www.vph-case.eu).

Declaration statements

Conflicts of interest: None.

Funding: This project has received funding from the European Union's Horizon 2020 research and innovation programme under the Marie Sklodowska-Curie grant agreement no. 642612, VPH-CaSE (www.vph-case.eu).

Ethical Approval: All data were collected at Bern University Hospital, following a protocol approved by the local ethics committee and the volunteers provided written informed consent (Swiss Adult Congenital Heart disease Registry, SACHER, ClinicalTrials.gov Identifier NCT 02258724).

References

[1] M. D. Reller, M. J. Strickland, T. Riehle-Colarusso, W. T. Mahle, A. Correa, Prevalence of congenital heart defects in metropolitan atlanta, 1998-2005, The Journal of pediatrics 153 (6) (2008) 807–813.

[2] J. I. Hoffman, S. Kaplan, The incidence of congenital heart disease, Journal of the American college of cardiology 39 (12) (2002) 1890–1900.

[3] H. Suradi, Z. M. Hijazi, Current management of coarctation of the aorta, Global Cardiology Science and Practice (2015) 44.

[4] H. Agrawal, J. W. Bokowski, D. Kenny, Coarctation of the aorta, Visual Guide to Neonatal Cardiology (2018) 260.

[5] M. L. Brown, H. M. Burkhart, H. M. Connolly, J. A. Dearani, F. Cetta, Z. Li, W. C. Oliver, C. A. Warnes, H. V. Schaff, Coarctation of the aorta: lifelong surveillance is mandatory following surgical repair, Journal of the American College of Cardiology 62 (11) (2013) 1020–1025.

[6] C. A. Warnes, R. G. Williams, T. M. Bashore, J. S. Child, H. M. Connolly, J. A. Dearani, P. del Nido, J. W. Fasules, T. P. Graham, Z. M. Hijazi, et al., Acc/aha 2008 guidelines for the management of adults with congenital heart disease: a report of the american college of cardiology/american heart association task force on practice guidelines (writing committee to develop guidelines on the management of adults with congenital heart disease) developed in collaboration with the american society of echocardiography, heart rhythm society, international society for adult congenital heart disease, society for cardiovascular angiography and interventions, and society of thoracic surgeons, Journal of the American College of Cardiology 52 (23) (2008) 143–263.

[7] E. by the Association for European Paediatric Cardiology (AEPC), A. F. Members, H. Baumgartner, P. Bonhoeffer, N. M. De Groot, F. de Haan, J. E. Deanfield, N. Galie, M. A. Gatzoulis, C. Gohlke-Baerwolf, et al., Esc guidelines for the management of grown-up congenital heart disease (new version 2010) the task force on the management of grown-up congenital heart disease of the european society of cardiology (esc), European heart journal 31 (23) (2010) 2915–2957.

[8] E. Beckmann, A. S. Jassar, Coarctation repair-redo challenges in the adults: what to do?, Journal of visualized surgery 4 (2018) 1–13.

[9] B. L. Seifert, K. DesRochers, M. Ta, G. Giraud, M. Zarandi, M. Gharib, D. J. Sahn, Accuracy of doppler methods for estimating peak-to-peak and peak instantaneous gradients across coarctation of the aorta: an in vitro study, Journal of the American Society of Echocardiography 12 (9) (1999) 744–753.

[10] J. J. Hom, K. Ordovas, G. P. Reddy, Velocity-encoded cine mr imaging in aortic coarctation: functional assessment of hemodynamic events, Radiographics 28 (2) (2008) 407–416.

[11] B. L. Wisotzkey, C. P. Hornik, A. S. Green, P. C. Barker, Comparison of invasive and non-invasive pressure gradients in aortic arch obstruction, Cardiology in the Young 25 (7) (2015) 1348–1357.

[12] F. Donati, S. Myerson, M. M. Bissell, N. P. Smith, S. Neubauer, M. J. Monaghan, D. A. Nordsletten, P. Lamata, Beyond bernoulli: improving the accuracy and precision of noninvasive estimation of peak pressure drops, Circulation: Cardiovascular Imaging 10 (1) (2017) e005207.

[13] I. Valverde, C. Staicu, H. Grotenhuis, A. Marzo, K. Rhode, Y. Shi, A. G. Brown, A. Tzifa, T. Hussain, G. Greil, et al., Predicting hemodynamics in native and residual coarctation: preliminary results of a rigid-wall computational-fluid-dynamics model (rw-cfd) validated against clinically invasive pressure measures at rest and during pharmacological stress, Journal of Cardiovascular Magnetic Resonance 13 (1) (2011) P49.

[14] J. F. LaDisa, C. A. Figueroa, I. E. Vignon-Clementel, H. J. Kim, N. Xiao, L. M. Ellwein, F. P. Chan, J. A. Feinstein, C. A. Taylor, Computational simulations for aortic coarctation: representative results from a sampling of patients, Journal of biomechanical engineering 133 (9) (2011) 0910081–9.

[15] J. S. Coogan, F. P. Chan, C. A. Taylor, J. A. Feinstein, Computational fluid dynamic simulations of aortic coarctation comparing the effects of surgical-and stent-based treatments on aortic compliance and ventricular workload, Catheterization and Cardiovascular Interventions 77 (5) (2011) 680–691.

[16] D. C. Wendell, M. M. Samyn, J. R. Cava, L. M. Ellwein, M. M. Krolikowski, K. L. Gandy, A. N. Pelech, S. C. Shadden, J. F. LaDisa, Including aortic valve morphology in computational fluid dynamic simulations: initial findings and application to aortic coarctation., Medical engineering and physics 35 (6) (2013) 12.

[17] S. Kwon, J. A. Feinstein, R. J. Dholakia, J. F. LaDisa, Quantitfication of local hemodynamic alterations caused by virtual implantation of three commercially-available stents for the treatment of aortic coarctation, Pediatric cardiology 35 (4) (2014) 732–740.

[18] L. Goubergrits, E. Riesenkampff, P. Yevtushenko, J. Schaller, U. Kertzscher, F. Berger, T. Kuehne, Is mri-based cfd able to improve clinical treatment of coarctations of aorta?, Annals of biomedical engineering 43 (1) (2015) 168–176.

[19] L. Goubergrits, E. Riesenkampff, P. Yevtushenko, J. Schaller, U. Kertzscher, A. Hennemuth, F. Berger, S. Schubert, T. Kuehne, MRI-based computational fluid dynamics for diagnosis and treatment prediction: Clinical validation study in patients with coarctation of aorta, Journal of Magnetic Resonance Imaging 41 (4) (2015) 909–916.

[20] D. Cosentino, C. Capelli, G. Derrick, S. Khambadkone, V. Muthurangu, A. M. Taylor, S. Schievano, Patient-specific computational models to support interventional procedures: a case study of complex aortic re-coarctation, EuroIntervention 11 (5) (2015) 669–672.

[21] Y. Zhu, R. Chen, Y.-H. Juan, H. Li, J. Wang, Z. Yu, H. Liu, Clinical validation and assessment of aortic hemodynamics using computational fluid dynamics simulations from computed tomography angiography, Biomedical engineering online 17 (1) (2018) 53.

[22] J. A. Sotelo, I. Valverde, P. B. Beerbaum, G. F. Greil, T. Schaeffter, R. Razavi, D. E. Hurtado, S. Uribe, C. A. Figueroa, Pressure gradient prediction in aortic coarctation using a computational-fluid-dynamics model: validation against invasive pressure catheterization at rest and pharmacological stress, Journal of Cardiovascular Magnetic Resonance 17 (1) (2015) Q78.

[23] K. Ralovich, L. M. Itu, D. Vitanovski, P. Sharma, R. I. Ionasec, V. Mihalef, W. Krawtschuk, Y. Zheng, A. D. Everett, G. Pongiglione, B. Leonardi, R. E. Ringel, N. Navab, T. Heimann, D. Comaniciu, Noninvasive hemodynamic assessment, treatment outcome prediction and follow-up of aortic coarctation from mr imaging., Medical physics 42 5 (2015) 2143–56.

[24] L. Itu, P. Sharma, K. Ralovich, V. Mihalef, R. Ionasec, A. Everett, R. Ringel, A. Kamen, D. Comaniciu, Non-invasive hemodynamic assessment of aortic coarctation: Validation with in vivo measurements, Annals of Biomedical Engineering 41 (4) (2013) 669–681.

[25] L. Antiga, M. Piccinelli, L. Botti, B. Ene-Iordache, A. Remuzzi, D. A. Steinman, An image-based modeling framework for patient-specific computational hemodynamics, Medical & biological engineering & computing 46 (11) (2008) 1097.

[26] A. Melis, R. H. Clayton, A. Marzo, Bayesian sensitivity analysis of a 1d vascular model with gaussian process

emulators, International journal for numerical methods in biomedical engineering 33 (12) (2017) e2882.

[27] K. S. Matthys, J. Alastruey, J. Peiró, A. W. Khir, P. Segers, P. R. Verdonck, K. H. Parker, S. J. Sherwin, Pulse wave propagation in a model human arterial network: assessment of 1-d numerical simulations against in vitro measurements, Journal of biomechanics 40 (15) (2007) 3476–3486.

[28] N. Stergiopulos, D. Young, T. Rogge, Computer simulation of arterial flow with applications to arterial and aortic stenoses, Journal of biomechanics 25 (12) (1992) 1477–1488.

[29] A. G. Brown, Y. Shi, A. Marzo, C. Staicu, I. Valverde, P. Beerbaum, P. V. Lawford, D. R. Hose, Accuracy vs. computational time: translating aortic simulations to the clinic, Journal of biomechanics 45 (3) (2012) 516–523.

[30] A. Avolio, Multi-branched model of the human arterial system, Medical and Biological Engineering and Computing 18 (6) (1980) 709–718.

[31] E.-S. H. Ibrahim, K. R. Johnson, A. B. Miller, J. M. Shaffer, R. D. White, Measuring aortic pulse wave velocity using high-field cardiovascular magnetic resonance: comparison of techniques, Journal of Cardiovascular Magnetic Resonance 12 (1) (2010) 26.

[32] J. Alastruey, K. H. Parker, S. J. Sherwin, et al., Arterial pulse wave haemodynamics (2012) 401–442.

[33] N. Xiao, J. Alastruey, C. Alberto Figueroa, A systematic comparison between 1-d and 3-d hemodynamics in compliant arterial models, International journal for numerical methods in biomedical engineering 30 (2) (2014) 204–231.

[34] M. Zamir, P. Sinclair, T. H. Wonnacott, Relation between diameter and flow in major branches of the arch of the aorta, Journal of biomechanics 25 (11) (1992) 1303–1310.

[35] J. Alastruey, K. Parker, J. Peiró, S. Sherwin, Lumped parameter outflow models for 1-d blood flow simulations: effect on pulse waves and parameter estimation, Communications in Computational Physics 4 (2) (2008) 317–336.

[36] J. Alastruey, T. Passerini, L. Formaggia, J. Peiró, Physical determining factors of the arterial pulse waveform: theoretical analysis and calculation using the 1-d formulation, Journal of Engineering Mathematics 77 (1) (2012) 19–37.

[37] J. Alastruey, N. Xiao, H. Fok, T. Schaeffter, C. A. Figueroa, On the impact of modelling assumptions in multi-scale, subject-specific models of aortic haemodynamics, Journal of The Royal Society Interface 13 (119) (2016) 20160073.

Table 1: Patient cohort classification: native, surgically repaired or hypoplastic descending aorta. Information about sex and age are reported for each case (average age: 32.89 ±14.66 years old, 55 % of males)

	Sex	**Age**	**Type**
Patient 1	male	28	native
Patient 2	female	59	native
Patient 3	female	20	hypoplastic descending aorta
Patient 4	male	21	surgically repaired (end-to-end anastomosis)
Patient 5	male	58	surgically repaired (patch repair)
Patient 6	female	34	surgically repaired (end-to-end anastomosis)
Patient 7	male	36	native
Patient 8	female	41	surgically repaired (end-to-end anastomosis)
Patient 9	female	25	native
Patient 10	male	22	native
Patient 11	male	18	surgically repaired (end-to-end anastomosis)

Table 2: Cuff pressure measurements for the 11 reported patients, systolic blood pressure, SBP, and diastolic blood pressure, DBP (NA = not available).

	SBP right arm	**DBP right arm**	**SBP leg**
Patient 1	152	85	130
Patient 2	125	75	95
Patient 3	131	60	100
Patient 4	134	66	120
Patient 5	147	95	120
Patient 6	150	83	115
Patient 7	138	69	110
Patient 8	167	75	NA
Patient 9	130	100	95
Patient 10	125	60	95
Patient 11	144	48	130

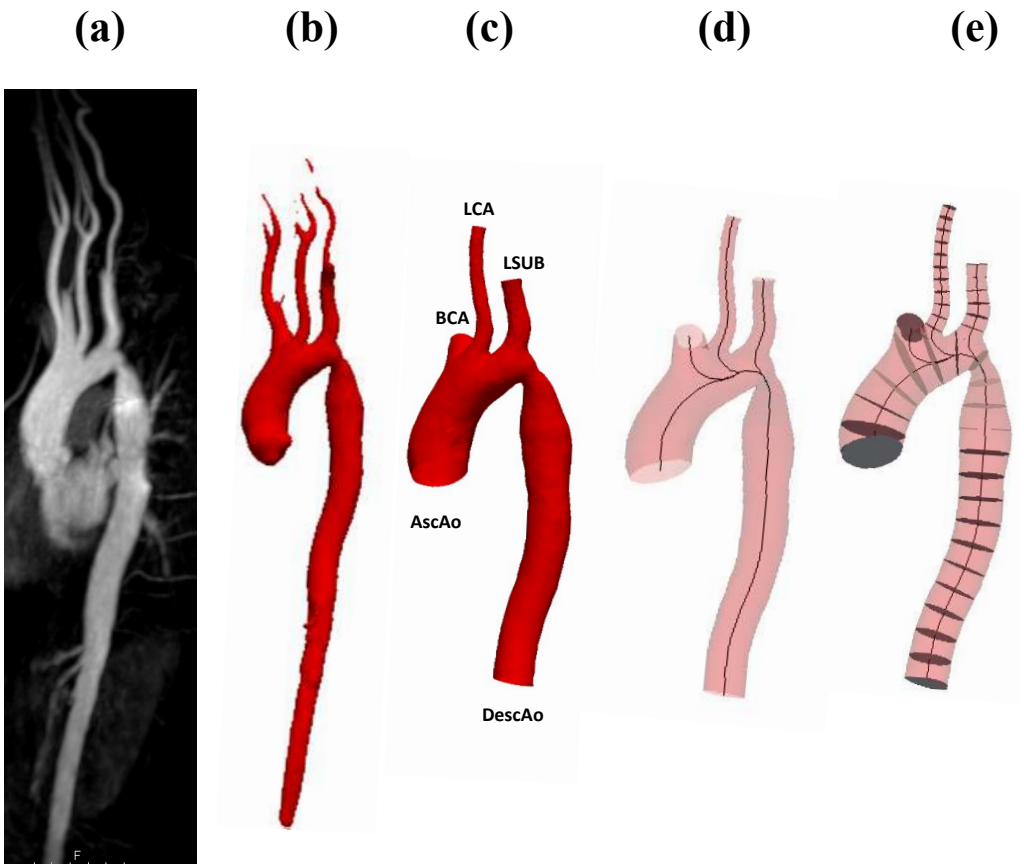

Figure 1: Patient-specific one dimensional and three-dimensional model construction. (a) Maximum intensity projection of the thoracic aorta from the contrast-enhanced magnetic resonance images (CE-MR). (b) 3D reconstructed geometry. (c) Post-processed 3D geometry (including surface smoothing) with truncation to obtain four outlets representing the ascending aorta, the descending aorta (truncated at the plane where MRI measurements were taken), the brachiocephalic artery (BCA), the left common carotid artery (LCA) and the left subclavian artery (LSUB). (d) Centreline and (e) cross-sectional area extraction used to define the segments of the 1D geometry.

Table 3: Foot-to-foot method parameters and resulting pulse wave velocity (c) derived for the 11 patients and the value used in the simulations.

	Δx **(m)**	Δt **(s)**	**c derived** $(m \cdot s^{-1})$	**c simulation** $(m \cdot s^{-1})$
Patient 1	0.359	0.0845	4.68	7
Patient 2	0.290	0.0263	11	11
Patient 3	0.231	0.0475	4.87	4.87
Patient 4	0.250	0.0538	4.64	6
Patient 5	0.296	0.0254	11.65	11.65
Patient 6	0.250	0.0501	4.99	6.5
Patient 7	0.280	0.0689	4.06	5.0
Patient 8	0.19	0.0218	8.70	8.70
Patient 9	0.3	0.0351	8.55	8.55
Patient 10	0.238	0.0218	10.9	10.9
Patient 11	0.250	0.0445	5.61	5.61

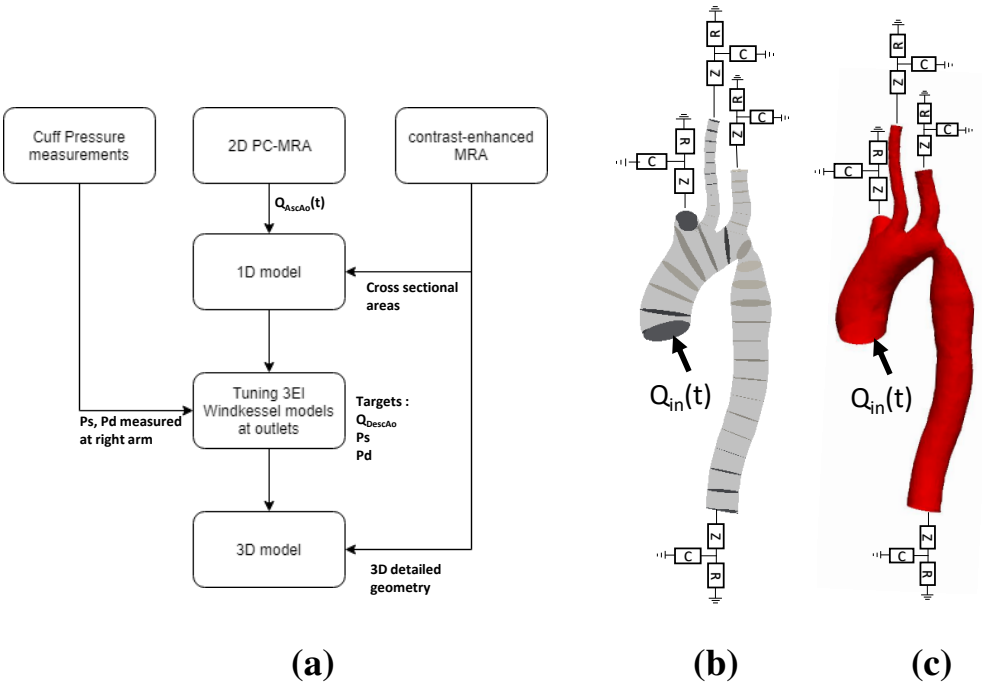

Figure 2: Schematic representing the multi-scale model domain and tuning process used to find the boundary conditions (BCs). (a) Flow chart representing the procedure used to find the WK parameters of the outflow BCs. (b) Schematic of the one-dimensional modelling approach: time-varying flow rate derived from 2D PC-MRI (Qin(t)) is directly applied at the inlet of the model and three-element Windkessel models are coupled at the outlets. The tuning process using the 1D model computes outflow Windkessel parameters for BCs based on mechanical properties derived from patient-specific available data. These parameters are then directly applied to the three-dimensional model imposing the same time-varying flow rate (Qin(t)) at the inlet and the same mechanical properties used for the one-dimensional model.

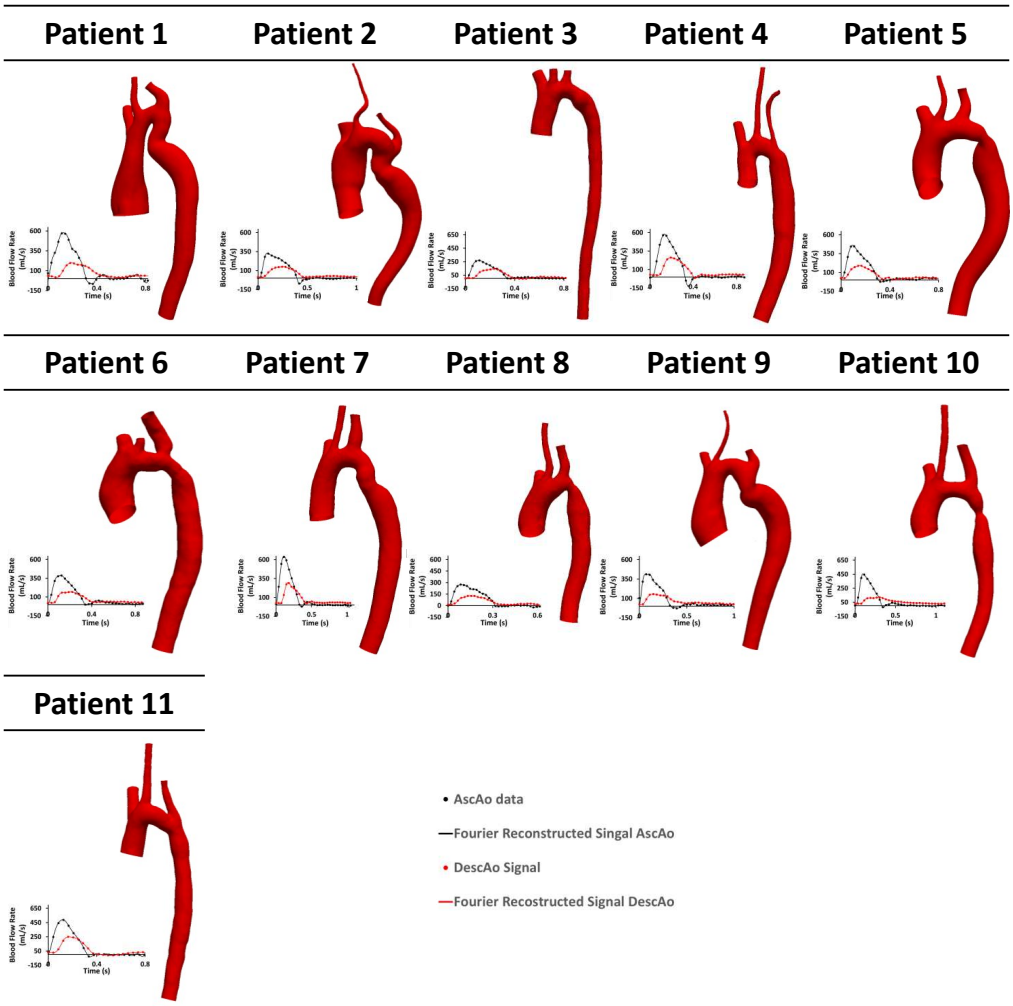

Figure 3: Segmented aortic anatomies extracted from MRA after the post processing and truncation step with aortic flow rates extracted from 2D PC-MRI data at the aortic root plane and diaphragmatic aortic plane, the original data had a temporal resolution of 20-30 phases per cardiac cycle, for the modelling approach the signal's temporal resolution was increased through a Fourier Series transformation.

Table 4: Degree of Stenosis reported for each of 11 patients in the cohort study. For patient 3 geometrical values were not reported as this case represents a hypoplastic descending aorta.

	Inlet diameter (mm)	**Reference diameter (mm)**	**Stenosis diameter (mm)**	**DS (%)**
Patient 1	45	21	18	10
Patient 2	29	29	23	36
Patient 4	21	23	15	59
Patient 5	29	27	14	79
Patient 6	26	23	13	68
Patient 7	23	20	16	22
Patient 8	27	18	10	69
Patient 9	32	26	16	45
Patient 10	24	14	8	72
Patient 11	24	17	15	23

Table 5: Effectiveness of the 1D/0D tuning strategy when compared with systolic and diastolic cuff pressure measurements and correspondence between the 1D/0D model and 3D/0D model in predicting ascending aortic pressures for the 11 cases. SBP refers to the systolic blood pressure, DBP refers to the diastolic blood pressure. Errors are reported in percentage (%).

	Measured		**1D/0D Tuned**		**No. iterations**	**Errors (%)**		**3D/0D Simulation**		**Errors (%)**	
	SBP	**DBP**	**SBP**	**DBP**		**SBP**	**DBP**	**SBP**	**DBP**	**SBP**	**DBP**
Patient 1	152	85	151	84	7	-1	-1	150	84	-1	-1
Patient 2	125	75	128	75	60	+2	0	130	77	+4	+3
Patient 3	131	60	131	60	3	0	0	128	60	-2	0
Patient 4	134	66	139	63	34	+4	-5	158	65	+18	+2
Patient 5	147	95	161	95	25	+10	0	166	100	+13	+5
Patient 6	150	83	150	83	4	0	0	162	78	+8	-6
Patient 7	138	69	138	69	8	0	0	142	70	+3	+1
Patient 8	167	75	167	75	5	0	0	169	79	+1	+5
Patient 9	130	100	156	81	35	+20	-19	177	86	+36	+14
Patient 10	125	60	164	61	34	+31	+2	195	69	+56	-15
Patient 11	144	48	145	48	9	-1	0	160	39	+11	-19

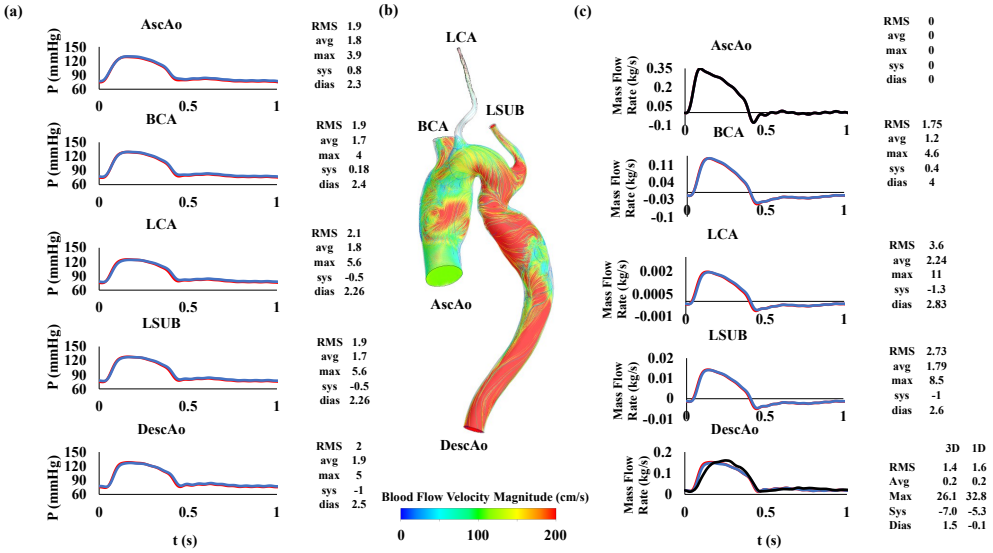

Figure 4: (a) Blood flow (Mass Flow Rate) and (c) Pressure (P) waveforms computed using the 1D (red lines) and 3D (blue lines) models at several locations: ascending aorta (AscAo), Brachiocephalic artery (BCA), left common carotid artery (LCA), left subclavian artery (LSUB) and descending aorta (DescAo) with comparison with available in-vivo data (black lines) for Patient 2. (b) velocity streamlines representing the velocity magnitude at systole.

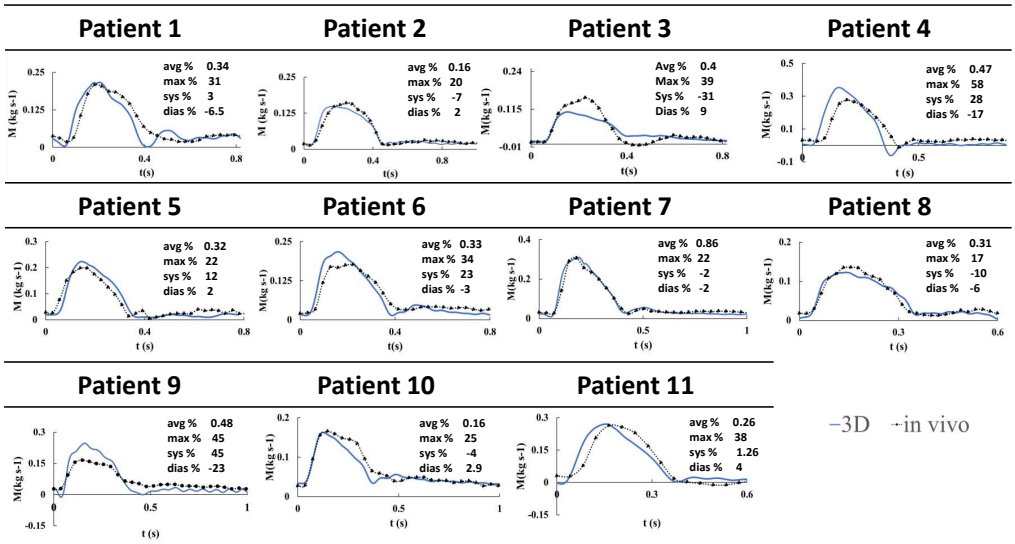

Figure 5: Comparison between computed and measured mass flow rate at the descending thoracic aorta (diaphragmatic level). CFD results extracted from 3D/0D models are presented with blue lines, while 2D PC-MRI data are shown by the black lines.

Table 6: Pressure gradients computed in the 3D/0D model, measured using the cuff arm-leg method and obtained from catheterization (NA= not available) reported in mmHg. Peak Reynolds number are reported at the coarctation site. Laminar (L) and turbulence SST model (T) are reported for the cases where the peak Reynolds number exceeds the limit imposed by the classical turbulence analysis (3500).

	peak Re	$Max_{AscAo} - Max_{DescAo}$		$Max_{gradient}$		$Sys_{gradient}$		$CoA_{gradient}$		Cuff arm-leg	Cath
					Native						
		L	T	L	T	L	T	L	T		
Patient 1	3405	1	-	35	-	18	-	9	-	22	32
Patient 2	1861	3	-	18	-	9	-	7	-	30	20
Patient 3	2948	15	-	39	-	20	-	20	-	31	31
Patient 7	5554	1	1	43	43	20	20	14	17	28	14
Patient 9	4341	15	16	47	48	24	24	22	18	35	34
Patient 10	5969	59	59	67	66	59	61	41	42	30	38
					Surgically Repaired						
		L	T	L	T	L	T	L	T		
Patient 4	6824	14	14	37	37	22	23	18	18	14	19
Patient 5	4617	9	9	33	33	24	23	23	22	27	23
Patient 6	4848	1	1	29	29	18	15	20	23	26	21
Patient 8	3482	4	-	23	-	20	-	21	-	NA	42
Patient 11	5031	2	1	38	36	23	16	8	12	14	30

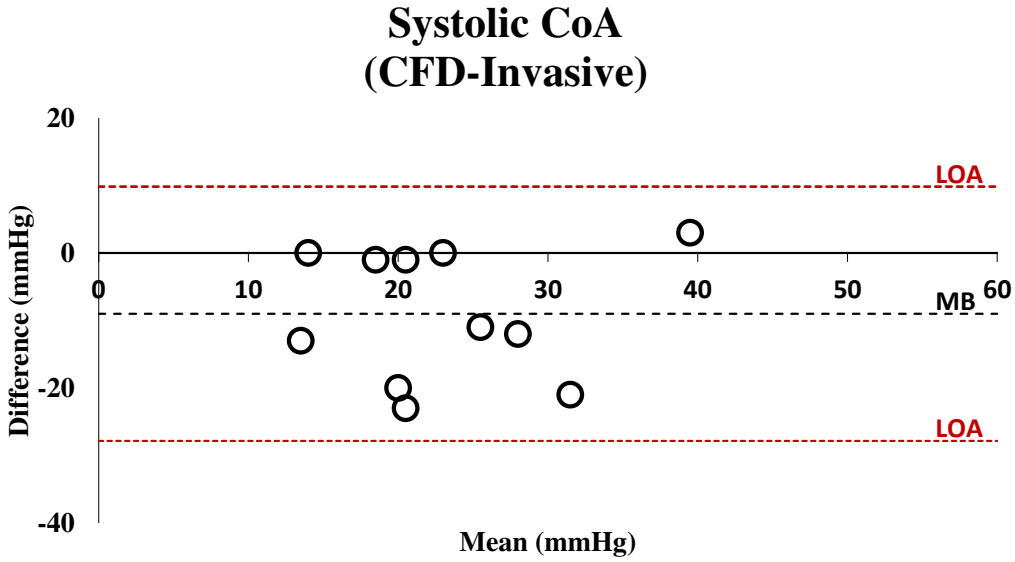

Figure 6: Bland-Altman plot: comparison of the invasive catheter measurement and computed CFD pressure gradient (mmHg) across the aortic coarctation for each case. Dashed red lines represent two standard deviations from the mean difference (LOA, 95 % limits of agreement) while the black dashed line represents the mean difference between the CFD and invasive data (MB).